Highly Efficient, Stable, and Ductile Ternary Nonfullerene Organic Solar Cells from a Two-Donor Polymer Blend

Huawei Hu, Long Ye, Masoud Ghasemi, Nrup Balar, Jeromy James Rech, Samuel J. Stuard, Wei You, Brendan T. O'Connor, and Harald Ade*

Organic solar cells (OSCs) are one of the most promising cost-effective options for utilizing solar energy, and, while the field of OSCs has progressed rapidly in device performance in the past few years, the stability of nonfullerene OSCs has received less attention. Developing devices with both high performance and long-term stability remains challenging, particularly if the material choice is restricted by roll-to-roll and benign solvent processing requirements and desirable mechanical durability. Building upon the ink (toluene:FTAZ:IT-M) that broke the 10% benchmark when blade-coated in air, a second donor material (PBDB-T) is introduced to stabilize and enhance performance with power conversion efficiency over 13% while keeping toluene as the solvent. More importantly, the ternary OSCs exhibit excellent thermal stability and storage stability while retaining high ductility. The excellent performance and stability are mainly attributed to the inhibition of the crystallization of nonfullerene small-molecular acceptors (SMAs) by introducing a stiff donor that also shows low miscibility with the nonfullerene SMA and a slightly higher highest occupied molecular orbital (HOMO) than the host polymer. The study indicates that improved stability and performance can be achieved in a synergistic way without significant embrittlement, which will accelerate the future development and application of nonfullerene OSCs.

Organic solar cells (OSCs) have attracted considerable attention as a future green technology to utilize solar energy due to their potential for large area fabrication on flexible substrates with low cost and environmentally friendly solution manufacturability.[1–3] Typical bulk heterojunction (BHJ) OSCs, consisting of

one donor and one acceptor as the photoactive layer, have achieved power conversion efficiencies (PCEs) over 13% in many systems due to the rapid development of high-performance organic materials, practically through the evolution of novel nonfullerene small molecular acceptors (SMAs) and matched polymer donors.[4–6] However, the use of binary OSCs often limits the range of light absorption and involves a complex phase separation dynamics that impacts device processing windows[4,7,8] and device stability.[9–11] To maximize the short-circuit current densities (J_{SC}) and overall device efficiencies, ternary OSCs have been developed. Ternary devices incorporate multiple materials similar to tandem solar cells, but with a single active layer similar to single junction OSCs, simplifying fabrication and relaxing the current matching constraint of tandem cells.[12–15] Recently, nonfullerene ternary OSCs based on two SMAs as the electron acceptors have received considerable interest owing to the strong absorptivity for wavelengths over 800 nm,[16] as well as the excellent compatibility of the two SMAs due to their very similar chemical structures.[17,18] By contrast, ternary OSCs consisting of two donor polymers usually result in relatively low performance because even small repulsive intermolecular interaction between the two polymer donors can lead to strong phase separation due to the limited entropy of polymers.[19–21] The morphology of nonfullerene SMAs can also be very sensitive to the choice of donor polymer.[22,23] Furthermore, most OSC studies focus primarily on the device performance and ignore the mechanical durability, which is an important consideration for OSC commercialization.

After considerable progress has been made on the development of high-performance nonfullerene OSCs, improvement in stability is of vital importance to guarantee a long operational lifetime.[10,24,25] The lifetime of an OSC is governed by the choice of photoactive layer, and can be limited by several possible origins, including exposure to humidity,[26] photooxidation of the BHJ layer and morphological instability due to spinodal demixing[9] or materials aggregation/crystallization under thermal stress,[27] and mechanical failure.[28] Most stability investigations to date have been focusing on fullerene-based OSCs,[10] and given the distinct difference between nonfullerene

Dr. H. Hu, Dr. L. Ye, Dr. M. Ghasemi, S. J. Stuard, Prof. H. Ade
Department of Physics and ORganic and Carbon
Electronics Labs (ORaCEL)
North Carolina State University
Raleigh, NC 27695, USA
E-mail: hwade@ncsu.edu
N. Balar, Prof. B. T. O'Connor
Department of Mechanical and Aerospace Engineering and ORaCEL
North Carolina State University
Raleigh, NC 27695, USA
J. J. Rech, Prof. W. You
Department of Chemistry
University of North Carolina at Chapel Hill
Chapel Hill, NC 27599, USA

The ORCID identification number(s) for the author(s) of this article can be found under https://doi.org/10.1002/adma.201808279.

and fullerene acceptors, the morphological stability of the non-fullerene SMA OCSs cannot be directly generalized from data on fullerene devices. In addition, simultaneous achievement of both high device performance and robust morphology stability remains a big challenge due to the difficulties in maintaining an optimal blend morphology under continuous operation even in harsh conditions.[10,29] Another important concern for future technology translations of OSCs is to utilize environmentally friendly solvent processing;[30,31] however, most high performance ternary OSCs are still processed from halogenated solvents[13,32] and achieving high-performance devices using nonhalogenated solvent systems remains a big challenge. Therefore, improving performance and stability at the same time is particularly constrained if the material choice is restricted by fabrication parameters such as roll-to-roll and benign solvent requirements. Such improvements are further constraint by needs to achieve and retain favorable mechanical properties such as high ductility, which is emerging as an important parameter.[33,34]

To address interconnected challenges relating to performance, morphological stablity, and mechanical stability, we report a highly efficient ternary OSC based on a combination of a nonfullerene acceptor (IT-M, the chemical structure is shown in **Figure 1**a) and two synergistic polymer donors (FTAZ and PBDB-T, also shown in Figure 1a) with complementary absorption, slightly different highest occupied molecular orbital (HOMO) energy levels, and differences in ductility. The choice was motivated by FTAZ:IT-M:toluene being the ink that broke the 10% benchmark when blade-coating in air from a single nonhalogenated solvent.[31] PBDB-T was chosen as a possibly stabilizing and performance enhancing donor due to

its ability to achieve high performance and excellent thermal stability in binary devices with a number of nonfullerene SMAs[35,36] and its smaller bandgap and slightly higher HOMO than FTAZ. The latter characteristics might enhance fill factor (FF) due to enhanced hole transport in high purity "highways."[37] The best efficiency of >13% was achieved in ternary OSCs with 20 wt% PBDB-T, processed from toluene (a halogen-free solvent) without additives and yielding an open circuit voltage (V_{OC}) of 0.95 V, a J_{SC} of 18.1 mA cm^{-2}, and a FF of 73.6%. This PCE exceeds that of the corresponding toluene-cast binary OSCs and is among the highest values for any ternary OSCs, including those cast from halogenated solvents.[15,20,37] The enhancement in PCE is mainly contributed by the increased device FF, which is attributed to reduced charge recombination and improved charge mobilities due to a favorable morphology and electronic landscape. Furthermore, we demonstrate that this nonfullerene ternary OSC system exhibits improved thermal stability and storage stability as well as favorable mechanical properties.

We first investigate the absorption properties of FTAZ, PBDB-T, and IT-M. Normalized ultraviolet–visible (UV–vis) absorption spectra and their corresponding absorbance and refractive index of FTAZ, PBDB-T, and IT-M neat films are shown in Figure 1b and Figure S1 (Supporting Information), respectively. Both donor polymers have complementary absorption with IT-M, and while there is some absorption spectral overlap between FTAZ and PBDB-T, the absorption peak of PBDB-T locates between that of FTAZ and IT-M. The absorption spectra of ternary and binary blend films composed of these materials are shown in Figure S1 (Supporting Information), suggesting a broad light absorption in the range of 400–800 nm.
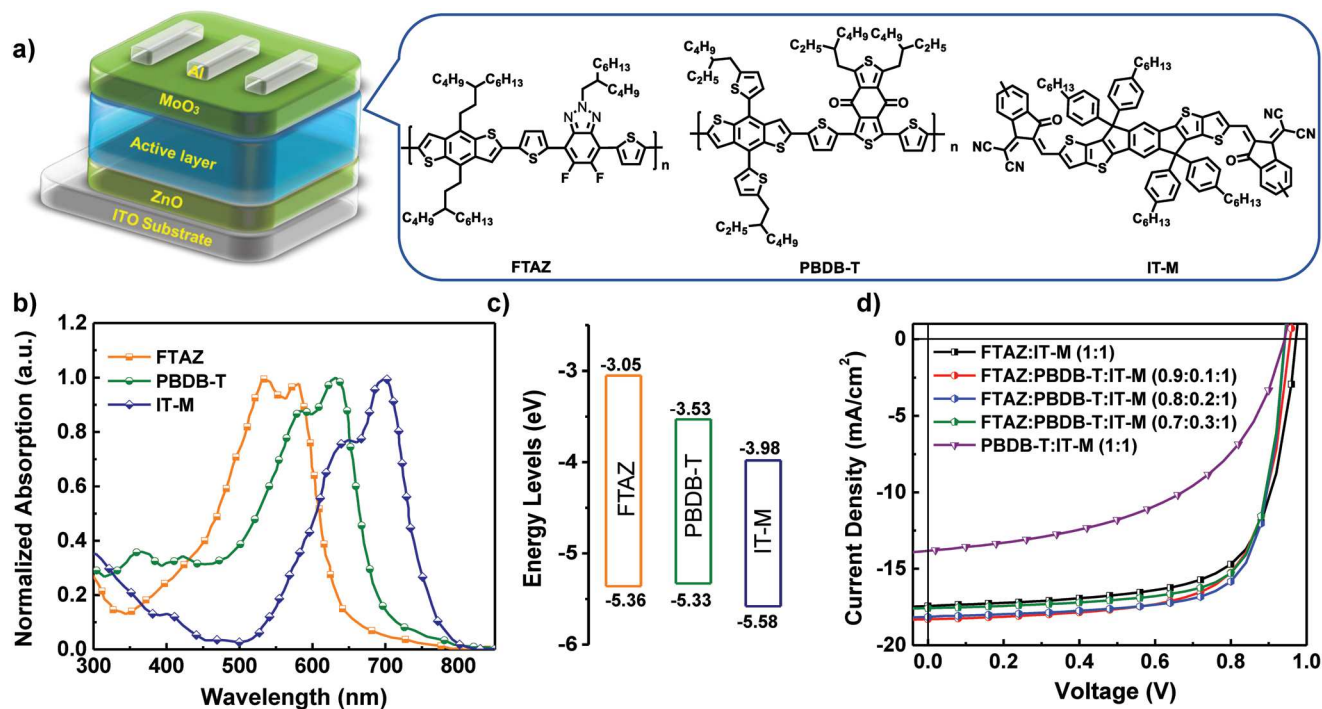
Figure 1. a) Schematic diagram of device structure and chemical structures of FTAZ, PBDB-T, and IT-M. b) Normalized UV–Vis absorption spectra and c) energy diagrams of the three materials. d) J–V characteristics of OSCs with different PBDB-T contents.

It is also noted that light harvesting from 600 to 660 nm can be enhanced with the increase of PBDB-T content, which can be well understood by the complementary absorption of neat PBDB-T film.[38,39] Besides the optimal light absorption of the ternary films, the V_{OC} of the ternary device should be slightly lower than that of the binary devices based on FTAZ:IT-M because of the slightly higher HOMO level of PBDB-T compared to FTAZ (Figure 1c).[31,40] The optimal amount of PBDB-T to add to the system should be based on balanced light harvesting, blend morphology, charge transport, and charge collection.

To obtain the optimized amount of PBDB-T in the ternary blend, nonfullerene OSCs were fabricated in an inverted device architecture (Figure 1a). According to our prior benchmark, the optimized processing condition for the FTAZ:IT-M based binary blade-coated solar cells cast without a solvent additive is the use of toluene with a donor/acceptor weight ratio of 1:1.[31] This condition was kept the same for all the binary and ternary combinations for a fair comparison and because of our goal was to improve the benchmark FTAZ:IT-M:toluene ink. That said, PBDB-T based binary devices can be improved with the use of additives when cast from nonhalogenated solvents.[41] The average device parameters from at least 10 devices are listed in **Table 1** and the current density–voltage (J–V) characteristics of the devices are shown in Figure 1d. The corresponding external quantum efficiency (EQE) spectra are shown in Figure S1d (Supporting Information). The binary nonfullerene OSC based on FTAZ:IT-M exhibits a PCE of 11.5% (11.8% max) with a V_{OC} of 0.96 V, a J_{SC} of 17.2 mA cm^{-2}, and an FF of 67.9%. On the other hand, the binary OSC based on PBDB-T:IT-M shows a similar V_{OC} of 0.94 V, but a comparatively lower PCE of 7.2% due to its relatively lower J_{SC} and FF of 13.5 mA cm^{-2} and 52.8%, respectively. The performance of the toluene-cast PBDB-T:IT-M binary films is comparable with the reported 7.9% efficiency when cast without additives from a halogen free solvent.[41] As summarized in Table 1, all the ternary solar cells show comparable V_{OC} values (between 0.94 and 0.96 V), but the FF is substantially increased with increasing the PBDB-T content and reaches 73.6% in the device with 20 wt% PBDB-T. However, further increasing the PBDB-T weight ratio leads to a decrease in the J_{SC} values and consequently low PCEs. In these ternary OSCs, FTAZ:PBDB-T:IT-M (0.8:0.2:1, weight ratio) exhibits the champion PCE of 13.2%, with a V_{OC} of 0.95 V, a J_{SC} of 18.1 mA cm^{-2}, and an FF of 73.6%, which is significantly

higher than the corresponding two binary OSCs. The calculated EQE values of the devices from Figure S1d (Supporting Information) are in good agreement with the J_{SC} values obtained from the J–V measurement.

To understand the impact of incorporating PBDB-T on the BHJ morphology, grazing incidence wide angle X-ray scattering (GIWAXS)[42] was performed to reveal the molecular packing and texture of the active layers. As observed from the GIWAXS profiles in **Figure 2** and Figure S2 in the Supporting Information, these blend films exhibit (010) peaks at $q_z = 1.75$ and 1.62 Å^{-1} in the out-of-plane direction for IT-M and FTAZ (Figure S3, Supporting Information), respectively. The corresponding out-of-plane (010) π–π coherence lengths (CL) of FTAZ and IT-M of these blend films were extracted via peak fitting by using the full width at half-maximum of the (010) stacking peaks. Figure 2e shows that both CLs increase for these blends with less than 20 wt% of PBDB-T and then decrease by adding 30 wt% of PBDB-T. Moreover, a peak at $q_z = 0.5$ Å^{-1} (Figure 2b), corresponding to the (100) lamellar stacking of IT-M, was observed in FTAZ:PBDB-T:IT-M (0.8:0.2:1) ternary blend film, which indicates strong molecular packing of IT-M in FTAZ:PBDB-T:IT-M (0.8:0.2:1) blend film. The strong molecular stacking is beneficial for charge transport in FTAZ:PBDB-T:IT-M (0.8:0.2:1) based solar cells,[43,44] which partially explains the highest FF achieved in the device. It is also noted that a peak at $q_{xy} = 0.62$ Å^{-1} (ascribed to the (001) peak of PBDB-T) is observed when PBDB-T is added into the active layer. It is thus inferred that PBDB-T possesses repulsive interactions and low miscibility with FTAZ and that these interactions influence the observed CL of FTAZ and IT-M in the ternary blends as a function of PBDB-T content. The charge mobilities, measured by space-charge-limited current (Table S1 and Figure S4, Supporting Information), are consistent with the GIWAXS results as the highest electron and hole mobilities of 4.62×10^{-4} and 3.95×10^{-4} cm^2 V^{-1} s^{-1}, respectively, are observed in FTAZ:PBDT-T:IT-M (0.8:0.2:1), which also corresponds to the highest FF for the corresponding ternary solar cells.

Resonant soft X-ray scattering (R-SoXS)[45] is employed to probe the composition correlation characteristics related to domain spacing and purity of these nonfullerene devices. Figure 2f illustrates the Lorentz corrected and thickness normalized circular R-SoXS profiles of these BHJ blends. Under the assumption of a globally isotropic 3D morphology in which the small molecule domains are essentially pure due to

Table 1. Photovoltaic parameters, standard deviation of the IT-M concentration, and long period of the nonfullerene OSCs with different PBDB-T content.

PBDB-T [donor wt%]	J_{SC} [mA cm^{-2}]	V_{OC} [V]	FF [%]	PCE[a] [%]	Relative σ[b] [±0.01]	$\sigma 2$[c] (high-q peak)	Long period [nm] Low-q	Long period [nm] High-q
0	17.2 ± 0.6	0.96 ± 0.01	67.9 ± 0.7	11.5 ± 0.3 (11.8)	0.88	0.16	25.1	19.0
10	18.2 ± 0.6	0.95 ± 0.01	70.0 ± 0.6	12.1 ± 0.3 (12.5)	0.95	0.24	28.9	19.6
20	18.1 ± 0.7	0.95 ± 0.01	73.6 ± 0.5	12.7 ± 0.4 (13.2)	0.97	0.40	31.4	19.6
30	17.5 ± 0.5	0.94 ± 0.01	72.5 ± 0.8	11.9 ± 0.3 (12.3)	1	0.28	34.9	20.9
100	13.5 ± 0.5	0.94 ± 0.01	52.8 ± 0.7	6.7 ± 0.4 (7.2)	0.65	0.20	41.9	20.3

[a]The best device efficiencies are provided in the parentheses; [b]The area of the R-SoXS profile over the q range probed is the integrated scattering intensity (ISI), with ISI$^{1/2}$ being proportional to the standard deviation, σ, of the IT-M concentration, which has been normalized relative to the highest value; [c]Relative σ for the high q peak.
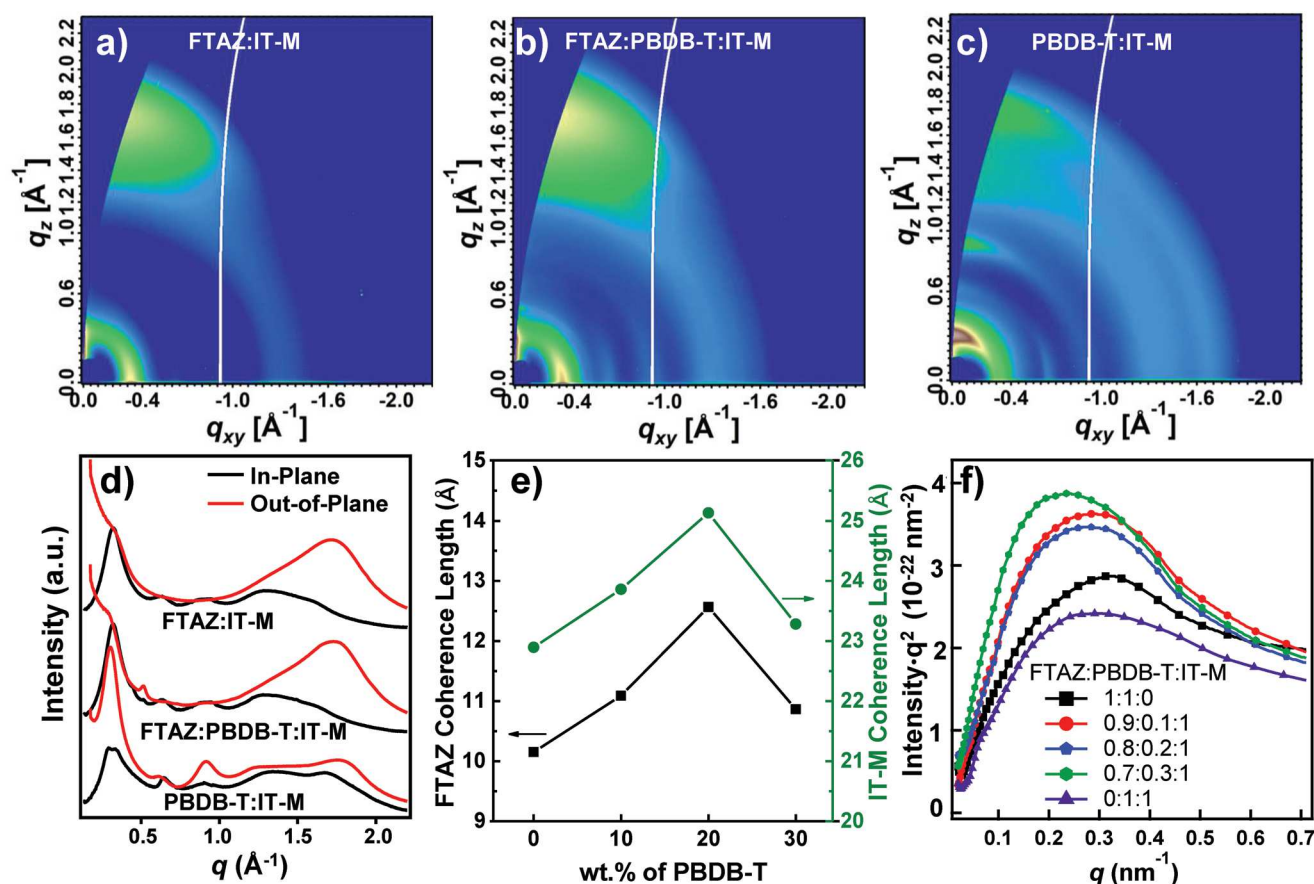
Figure 2. a–c) 2D GIWAXS patterns and d) 1D profiles of films based on FTAZ:IT-M (1:1), FTAZ:PBDB-T:IT-M (0.8:0.2:1), and PBDB-T:IT-M (1:1), respectively. e) Out-of-plane π–π coherence lengths of FTAZ and IT-M. f) Thickness and Lorentz-corrected R-SoXS profiles of blend films.

the low molecular weight,[4,8,46] the root-mean-square standard deviation, σ, of the IT-M concentration is proportional to the square root of the normalized integrated scattering intensity (ISI) and relates monotonically to the average IT-M concentration in the polymer rich domains.[4] The relative IT-M standard deviations quantified from R-SoXS measurement are listed in Table 1, where ternary blends based on FTAZ:PBDB-T:IT-M (0.7:0.3:1) and FTAZ:PBDB-T:IT-M (0.8:0.2:1) exhibit relatively higher σ of 1 and 0.97, respectively. The higher σ is critical in helping to suppress bimolecular recombination as well as promoting charge collection, leading to improved device FF as long as the IT-M concentration is above the percolation limit.[4,47] As the FF does not completely correlate to σ derived from all length scales probed, we fit the R-SoXS scattering profiles with two log-normal peaks (Figure S4, Supporting Information). The low-q peaks for the ternary blends slightly shift toward lower q (from 0.25 to 0.18 nm^{-1}) with the increased content of PBDB-T, indicating that a relatively larger long period is obtained with higher content of PBDB-T. By contrast, the high-q peaks of FTAZ-based films are located at fixed q at $\approx$0.32 nm^{-1} for binary and ternary blends, corresponding to a long period of the domains of $\approx$20 nm, which matches well with the typical exciton diffusion length. When considering the domain purities by analyzing the scattering intensity and standard deviation of the composition, the FTAZ:PBDB-T:IT-M (0.8:0.2:1) blend exhibits

the largest IT-M standard deviation at the smallest length scales (see Table 1), which agrees well with previous results that established the importance of achieving a high σ (i.e., high purity) at length scales corresponding to the exciton diffusion length.[48,49] Interpreting the R-SoXS further is complex, as is the case with all ternary systems. Assumptions about kinetic and thermodynamic factors have to be made frequently. We will return to this topic below after we acquire thermodynamic inferences about miscibility. Furthermore, the influence of adding PBDB-T on charge recombination was investigated with light intensity dependent J_{SC} measurement as function of bias voltage (Figure S5, Supporting Information). The smaller scaling exponent (α) for all bias conditions and the dramatic drop of it near V_{OC} suggests stronger bimolecular recombination in FTAZ:IT-M binary devices compared to the optimized ternary.

Overall, the molecular packing derived from GIWAXS and the domain purity data from R-SoXS explain the increase in FF due to increased extraction from higher mobility and the reduction of bimolecular recombination by reducing the number of dispersed D/A sites. The improvement in FF, combined with the information about HUMO–LUMO levels and the V_{OC}, implies that the holes get trapped in PBDB-T domains that result in reduced bimolecular recombination due to a lower IT-M concentration relative to the FTAZ domains. This scenario is also consistent with an interpretation of the R-SoXS resulting

ADVANCED
SCIENCE NEWS
www.advancedsciencenews.com

ADVANCED
MATERIALS
www.advmat.de

that the PBDB-T domains are purer than the FTAZ domains in concentrations up to 20% PDBD-T. To confirm that higher IT-M purity in PBDB-T is a thermodynamically favored morphology, we employ differential scanning calorimetry (DSC) measurement to investigate the qualitative miscibility between IT-M and the two polymer donors. As shown in the DSC curves in Figure S6 (Supporting Information), IT-M does not show any melting peak (due to sublimation) but exhibits pronounced exothermal peaks in the first heating cycle corresponding to cold-crystallization of the vitrified, amorphous volume fraction of the material.[50] Compared with the pristine IT-M, it is clear that the cold crystallization peak of FTAZ:IT-M blends is broadened and substantially more suppressed than that of PBDB-T:IT-M blends. This indicates lower miscibility of IT-M in PBDB-T than IT-M in FTAZ.[4] The increase in the standard deviation of the IT-M distribution and domain spacing upon the addition of PBDB-T into FTAZ:IT-M is consistent with the lower miscibility between PBDB-T and IT-M.[8] The stronger repulsive interaction with IT-M for PBDB-T leads to stronger liquid–liquid phase separation and larger domains at the larger length-scale.[7,49] The stronger repulsive interaction for PBDB-T also likely leads to purer domains relative to the FTAZ, irrespective of whether the devices overall are likely not processed to equilibrium but quenched.[7,9,51] We note that the devices can reach

local equilibrium most readily at the small length scale, which is where we observe the largest IT-M standard deviation and thus average domain purity. As a result, the mechanism for improved device performance is likely due to preferential transport of the hole polarons in the more pure PBDB-T network that acts like a highway as previously inferred in a fullerene based model system.[37] Here, we explicitly delineate the thermodynamic drivers that cause such a favorable morphology.

Having been able to improve the photovoltaic performance with the addition of PBDB-T motivated us to investigate the relative device stability of our binary and ternary OSCs. We compared the thermal stabilities of FTAZ:IT-M (1:1) and FTAZ:PBDB-T:IT-M (0.8:0.2:1) and PBDB-T:IT-M (1:1) based devices. After thermal stress at 180 °C for 10 min, the FTAZ:IT-M binary device only gives a PCE of 6.2% (**Figure 3**a; Table S2, Supporting Information), which shows a dramatic efficiency loss of ≈46% under this thermal stress. The PCE loss is a result of decreases in all three photovoltaic parameters, indicating a distinct phase organization at such a high annealing temperature.[28] This is evidenced by the morphology changes, GIWAXS patterns clearly exhibit multiple peaks in FTAZ:IT-M blend film after thermal annealing (Figure 3c), indicating the crystallization of IT-M in the blend films upon thermally annealed at 180 °C. To support the conclusion that IT-M can crystallize, optical microscopy images exhibit
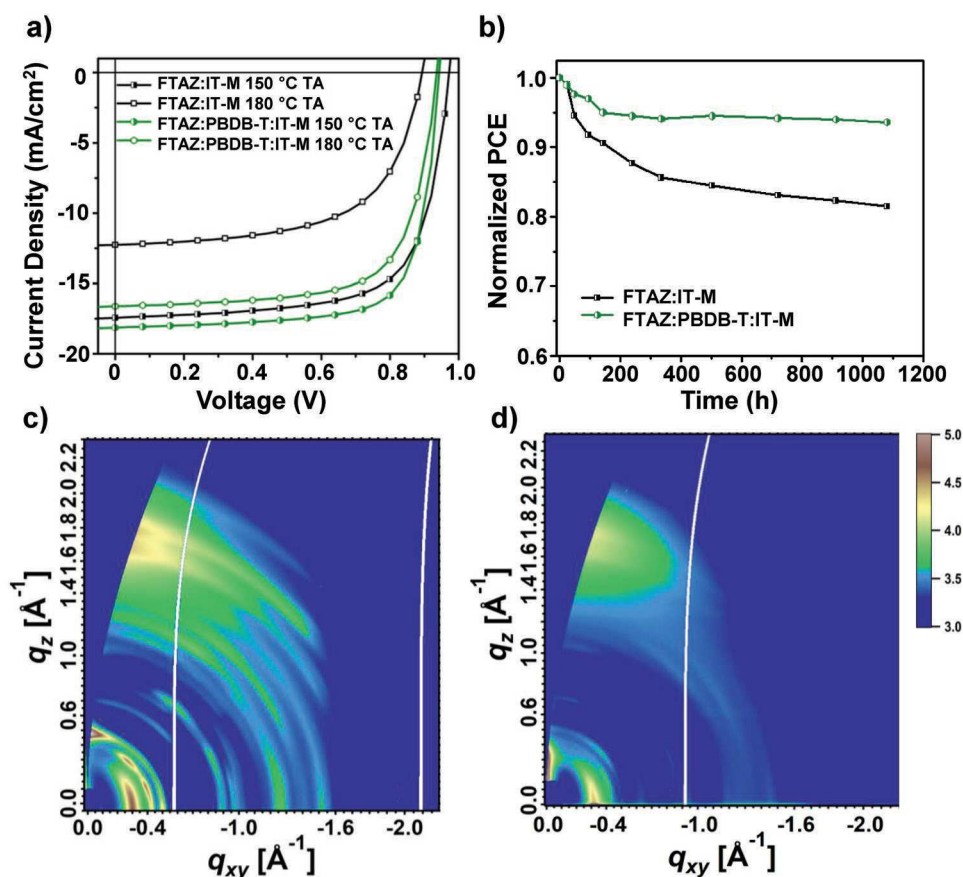
Figure 3. Device stability of nonfullerene OSCs. a) *J–V* characteristics of devices based on FTAZ:IT-M (1:1) and FTAZ:PBDB-T:IT-M (0.8:0.2:1) thermally annealed (TA) at elevated temperatures for 10 min. b) Normalized PCE of devices based on FTAZ:IT-M (1:1) and FTAZ:PBDB-T:IT-M (0.8:0.2:1) (annealed at 150 °C for 10 min) as a function of storage time in the nitrogen under dark. c,d) 2D GIWAXS patterns of FTAZ:IT-M (1:1) and FTAZ:PBDB-T:IT-M (0.8:0.2:1) based blend films annealed at 180 °C.

micrometer-sized crystals after thermal annealing at 180 °C for FTAZ:IT-M based blend films (see Figure S7, Supporting Information). This is very similar to many fullerene-based OSCs, where thermally induced fullerene aggregation or crystallization has been identified as the key mechanism for the PCE loss.[11,52] By contrast, the material crystallization behavior has been significantly suppressed for the corresponding ternary blend film with 20 wt% PBDB-T even after thermal annealing at 180 °C (Figure 3d). In addition, the R-SoXS profiles of the FTAZ:IT-M films (Figure S8, Supporting Information) indicate that the IT-M standard deviation decreased from 0.88 of 150 °C annealed films to 0.78 for 180 °C annealed ones, and the low-q peak shift to ≈0.02 nm^{-1} (Figure S9, Supporting Information), which should be attributed to reduced IT-M concentration in mixed domains due to the extra chemical potential of the IT-M crystals and larger domains size due to coarsening, respectively. The incorporation of PBDB-T prevented such a significant morphological change under higher thermal stress (the IT-M standard deviation decreases only from 0.97 to 0.92 and the long period of low-q and high-q increases marginally from 31.4 and 19.6 nm to 34.9 and 20.9 nm, respectively). As a result, we can still get ≈86% of the efficiency achieved from the reference devices annealed at 150 °C (see Figure 3a). The stability is comparable to that of binary PBDB-T:IT-M, where the devices annealed at 180 °C get ≈90% of the efficiency achieved from 150 °C annealed OSCs (Table S2, Supporting Information). We note that this direct comparison of the binary shows that the binary PBDB-T:IT-M devices are more stable than binary FTAZ:IT-M device. We then compared the shelf-life stability of these FTAZ-based OSCs. Normalized PCE of the devices as a function of storage time is shown in Figure 3b. FTAZ:IT-M binary solar cells attained 80% of the initial PCE after a storage time of ≈1000 h in a glovebox (Table S3 and Figure S10, Supporting Information). Ternary devices with 20 wt% PBDB-T still get over 90% of the initial efficiency (PCE = 12.7%) and are 10% higher than the beginning binary efficiency of 11.5%. Furthermore, we note that visual extrapolation of the stability data indicates that the ternary device has reached stable performance at ≈400 h, whereas the binary likely continues to decline beyond 1000 h. Overall, these results clearly indicate that solar cells based on the FTAZ:PBDB-T:IT-M (0.8:0.2:1) ternary not only exhibit superior shelf-life stability but also show substantially improved resistance to thermal stress compared to FTAZ:IT-M binary devices.

In order to elucidate the reason for the improved stability of the ternary compared to the FTAZ:IT-M binary and because mechanical properties also play a crucial role in roll-to-roll fabrication and are important for eventual OSC technological deployment, we further measured the crack onset strain (COS) of the two binaries and the optimized ternary blends (Figure S11, Supporting Information). Here, COS captures film ductility, and we use it as a simple screening tool for mechanical behavior. COS has been shown to correlate well with cohesion and toughness in organic semiconductor neat and blend films,[53–55] all of which are important parameters for mechanical reliability.[34] FTAZ:IT-M (1:1) and FTAZ:PBDB-T:IT-M (0.8:0.2:1) based blend films exhibit comparable good ductility with the COS of 33 ± 5% and 29 ± 5%, respectively. By contrast, the PBDB-T:IT-M (1:1) binary blend film exhibits a low crack onset strain of only 10 ± 3%. It should be noted that the ductility is dependent on the molecular weight of the polymers as well as its molecular structure. The molecular weight of PBDB-T

(M_n ≈ 30 kDa) is lower than that of FTAZ (M_n ≈ 60 kDa), and this may contribute to PBDB-T being more brittle. In our comparative study, that dependence on molecular weight is not important, only the existence of an absolute difference and its exploitation matter. Compared with the COS of binary blend based on host FTAZ polymer, the ductility of ternary blend was not affected much with 20 wt% PBDB-T. We also note that these values are for films on UV/ozone-treated poly(dimethylsiloxane) (PDMS) substrates, which are used to increase and magnify the differences in measured COS. Nevertheless, the film COS of the ternary systems are comparable to reports of all-polymer systems, which are often lauded for their ductility.[34,53,54] The PBDB-T likely leads to lower the diffusion of IT-M due to the more rigid nature of the polymer chains that is implied by its lower ductility.[34,52,56] This then suppresses the ability of the IT-M to crystallize as observed in GIWAXS (Figure 3). The revealed mechanical property and stability relation are rather illuminating. This relation is significant because it indicates that there is a possible general engineering constraint in the development and use of OSCs: For binary OSCs, the more ductile and stretchable active layers are likely more unstable than the more brittle active layers, a conclusion that warrants additional detailed studies. Reaching high performance in both parameters in binary devices will be very challenging, but the ternary strategy presented here indicates that improved stability and performance can be achieved in a synergistic way without much impact on ductility.

Finally, we explored the general scope of the ternary stabilization strategy using other nonfullerene SMAs. Nonfullerene ternary solar devices based on a structurally similar acceptor ITIC (structure shown in Figure S12a, Supporting Information) and FTAZ with 20 wt% PBDB-T were fabricated. A higher PCE of 11.0% (Figure S12b, Supporting Information) of the ternary device than the PCE (10.4%) of binary device based on FTAZ:ITIC was achieved. Furthermore, ternary OSCs achieved a PCE of 8.8% after being thermally annealed at 180 °C for 10 min, while the corresponding FTAZ:ITIC devices only get a PCE of 5.8% (Figure S12b and Table S4, Supporting Information). In addition, another well-known nonfullerene SMA (EH-IDTBR, structure shown in Figure S12a, Supporting Information) was also used to test the applicable scope of the ternary system. Ternary solar cell (annealed at 80 °C for 10 min) based on this film (10.0%, Figure S12c and Table S4, Supporting Information) showed slightly improved performances to the control devices based on FTAZ:EH-IDTBR (9.8%) blend films. Importantly, the PCE of the binary FTAZ:EH-IDTBR drops to 8.0% and 4.0% under higher annealing temperatures at 120 and 140 °C, respectively, while the corresponding ternary solar cells can still obtain promising PCE of 10.0% and 8.8%, respectively. The encouraging results clearly support the wide-ranging applicability to achieve a stable OSC by incorporating an incompatible brittle polymer that also exhibits low miscibility with the nonfullerene SMA.

In summary, we report high efficiency, moderately ductile, and relatively stable nonfullerene ternary OSCs by integrating two polymer donors FTAZ and PBDB-T and one SMA IT-M with an additive-free and halogen-free processing method. A PCE over 13% can be achieved for ternary OSCs having a weight ratio of 0.8:0.2:1 for FTAZ:PBDB-T:IT-M, which is

**ADVANCED
SCIENCE NEWS**
www.advancedsciencenews.com

**ADVANCED
MATERIALS**
www.advmat.de

among the highest values for nonfullerene ternary solar cells based on dual donors. The enhancement in device performance of the ternary OSCs is mainly attributed to the enhancement of device FF, which is due to the reduced charge recombination in the highly pure minority donor phase that traps the holes into its network and improved charge mobilities. More importantly, the ternary system demonstrates good mechanical ductility, superior shelf-life stability, and excellent thermal stress tolerance. The excellent performance under high thermal stress is mainly attributed to the inhibition of nonfullerene SMA crystallization by introducing a stiff polymer (PBDB-T). The results indicate that synergistic enhancements can be achieved in more than one parameter. Given that the toluene:FTAZ:IT-M ink achieved excellent results previously by blade-coating in air, we expect the ternary improvements achieved here to also translate to blade-coating and other R2R compatible methods. The desirable design characteristics of the minority donor can be summarized as follows: i) it should be more immiscible with the nonfullerene than the host majority donor to form purer mixed domains than the host, ii) it should have a slightly higher HOMO than the host to trap and preferentially transport the holes, and iii) it should be less ductile and more brittle than the host. This work provides a simple yet effective approach toward highly efficient ternary OSCs with excellent thermal stability and mechanical properties, which would potentially be used to accelerate the future application of nonfullerene OSCs.

Supporting Information

Supporting Information is available from the Wiley Online Library or from the author.

Acknowledgements

Conflict of Interest

The authors declare no conflict of interest.

Keywords

[1] Y. Huang, E. J. Kramer, A. J. Heeger, G. C. Bazan, *Chem. Rev.* **2014**, *114*, 7006.

[2] L. Lu, T. Zheng, Q. Wu, A. M. Schneider, D. Zhao, L. Yu, *Chem. Rev.* **2015**, *115*, 12666.

[3] G. Zhang, J. Zhao, P. C. Y. Chow, K. Jiang, J. Zhang, Z. Zhu, J. Zhang, F. Huang, H. Yan, *Chem. Rev.* **2018**, *118*, 3447.

[4] L. Ye, H. Hu, M. Ghasemi, T. Wang, B. A. Collins, J. H. Kim, K. Jiang, J. H. Carpenter, H. Li, Z. Li, T. McAfee, J. Zhao, X. Chen, J. L. Y. Lai, T. Ma, J. L. Bredas, H. Yan, H. Ade, *Nat. Mater.* **2018**, *17*, 253.

[5] C. Sun, F. Pan, H. Bin, J. Zhang, L. Xue, B. Qiu, Z. Wei, Z. G. Zhang, Y. Li, *Nat. Commun.* **2018**, *9*, 743.

[6] C. Yan, S. Barlow, Z. Wang, H. Yan, A. K. Y. Jen, S. R. Marder, X. Zhan, *Nat. Rev. Mater.* **2018**, *3*, 18003.

[7] L. Ye, S. Li, X. Liu, X. Zhang, M. Ghasemi, Y. Xiong, J. Hou, H. Ade, *Joule* **2019**, *3*, 443.

[8] L. Ye, B. A. Collins, X. jiao, J. Zhao, H. Yan, H. Ade, *Adv. Energy Mater.* **2018**, *8*, 1703058.

[9] N. Li, J. D. Perea, T. Kassar, M. Richter, T. Heumueller, G. J. Matt, Y. Hou, N. S. Guldal, H. Chen, S. Chen, S. Langner, M. Berlinghof, T. Unruh, C. J. Brabec, *Nat. Commun.* **2017**, *8*, 14541.

[10] P. Cheng, X. Zhan, *Chem. Soc. Rev.* **2016**, *45*, 2544.

[11] W. R. Mateker, M. D. McGehee, *Adv. Mater.* **2017**, *29*, 1603940.

[12] L. Lu, T. Xu, W. Chen, E. S. Landry, L. Yu, *Nat. Photonics* **2014**, *8*, 716.

[13] D. Baran, R. S. Ashraf, D. A. Hanifi, M. Abdelsamie, N. Gasparini, J. A. Rohr, S. Holliday, A. Wadsworth, S. Lockett, M. Neophytou, C. J. Emmott, J. Nelson, C. J. Brabec, A. Amassian, A. Salleo, T. Kirchartz, J. R. Durrant, I. McCulloch, *Nat. Mater.* **2017**, *16*, 363.

[14] Y. Yang, W. Chen, L. Dou, W.-H. Chang, H.-S. Duan, B. Bob, G. Li, Y. Yang, *Nat. Photonics* **2015**, *9*, 190.

[15] P. Cheng, J. Wang, Q. Zhang, W. Huang, J. Zhu, R. Wang, S. Y. Chang, P. Sun, L. Meng, H. Zhao, H. W. Cheng, T. Huang, Y. Liu, C. Wang, C. Zhu, W. You, X. Zhan, Y. Yang, *Adv. Mater.* **2018**, *30*, 1801501.

[16] H. Yao, Y. Cui, R. Yu, B. Gao, H. Zhang, J. Hou, *Angew. Chem., Int. Ed.* **2017**, *56*, 3045.

[17] R. Yu, S. Zhang, H. Yao, B. Guo, S. Li, H. Zhang, M. Zhang, J. Hou, *Adv. Mater.* **2017**, *29*, 1700437.

[18] X. Ma, W. Gao, J. Yu, Q. An, M. Zhang, Z. Hu, J. Wang, W. Tang, C. Yang, F. Zhang, *Energy Environ. Sci.* **2018**, *11*, 2134.

[19] M. Ghasemi, L. Ye, Q. Zhang, L. Yan, J. H. Kim, O. Awartani, W. You, A. Gadisa, H. Ade, *Adv. Mater.* **2017**, *29*, 1604603.

[20] W. Huang, P. Cheng, Y. M. Yang, G. Li, Y. Yang, *Adv. Mater.* **2018**, *30*, 1705706.

[21] J.-H. Kim, C. Schaefer, T. Ma, J. Zhao, J. Turner, M. Ghasemi, I. Constantinou, F. So, H. Yan, A. Gadisa, H. Ade, *Adv. Energy Mater.* **2018**, *8*, 1802293.

[22] Y. Lin, F. Zhao, Y. Wu, K. Chen, Y. Xia, G. Li, S. K. Prasad, J. Zhu, L. Huo, H. Bin, Z. G. Zhang, X. Guo, M. Zhang, Y. Sun, F. Gao, Z. Wei, W. Ma, C. Wang, J. Hodgkiss, Z. Bo, O. Inganas, Y. Li, X. Zhan, *Adv. Mater.* **2017**, *29*, 1604155.

[23] H. Hu, K. Jiang, P. C. Y. Chow, L. Ye, G. Zhang, Z. Li, J. H. Carpenter, H. Ade, H. Yan, *Adv. Energy Mater.* **2018**, *8*, 1701674.

[24] M. Jorgensen, K. Norrman, S. A. Gevorgyan, T. Tromholt, B. Andreasen, F. C. Krebs, *Adv. Mater.* **2012**, *24*, 580.

[25] K. Zhang, R. Xia, B. Fan, X. Liu, Z. Wang, S. Dong, H. L. Yip, L. Ying, F. Huang, Y. Cao, *Adv. Mater.* **2018**, *30*, 1803166.

[26] H. Klumbies, M. Karl, M. Hermenau, R. Rösch, M. Seeland, H. Hoppe, L. Müller-Meskamp, K. Leo, *Sol. Energy Mater. Sol. Cells* **2014**, *120*, 685.

[27] B. J. Kim, Y. Miyamoto, B. Ma, J. M. J. Fréchet, *Adv. Funct. Mater.* **2009**, *19*, 2273.

[28] M. Jørgensen, K. Norrman, F. C. Krebs, *Sol. Energy Mater. Sol. Cells* **2008**, *92*, 686.

ADVANCED
SCIENCE NEWS

www.advancedsciencenews.com

**ADVANCED
MATERIALS**

www.advmat.de

[29] X. Xu, K. Fukuda, A. Karki, S. Park, H. Kimura, H. Jinno, N. Watanabe, S. Yamamoto, S. Shimomura, D. Kitazawa, T. Yokota, S. Umezu, T. Q. Nguyen, T. Someya, *Proc. Natl. Acad. Sci. USA* **2018**, *115*, 4589.

[30] J. Zhao, Y. Li, G. Yang, K. Jiang, H. Lin, H. Ade, W. Ma, H. Yan, *Nat. Energy* **2016**, *1*, 15027.

[31] L. Ye, Y. Xiong, Q. Zhang, S. Li, C. Wang, Z. Jiang, J. Hou, W. You, H. Ade, *Adv. Mater.* **2018**, *30*, 1705485.

[32] Y. Xie, F. Yang, Y. Li, M. A. Uddin, P. Bi, B. Fan, Y. Cai, X. Hao, H. Y. Woo, W. Li, F. Liu, Y. Sun, *Adv. Mater.* **2018**, *30*, 1803045.

[33] D. J. Lipomi, *Joule* **2018**, *2*, 195.

[34] S. E. Root, S. Savagatrup, A. D. Printz, D. Rodriquez, D. J. Lipomi, *Chem. Rev.* **2017**, *117*, 6467.

[35] W. Zhao, D. Qian, S. Zhang, S. Li, O. Inganas, F. Gao, J. Hou, *Adv. Mater.* **2016**, *28*, 4734.

[36] S. Li, L. Zhan, F. Liu, J. Ren, M. Shi, C. Z. Li, T. P. Russell, H. Chen, *Adv. Mater.* **2018**, *30*, 1705208.

[37] N. Gasparini, X. Jiao, T. Heumueller, D. Baran, G. J. Matt, S. Fladischer, E. Spiecker, H. Ade, C. J. Brabec, T. Ameri, *Nat. Energy* **2016**, *1*, 16118.

[38] M. Xiao, K. Zhang, S. Dong, Q. Yin, Z. Liu, L. Liu, F. Huang, Y. Cao, *ACS Appl. Mater. Interfaces* **2018**, *10*, 25594.

[39] H. Lin, S. Chen, Z. Li, J. Y. Lai, G. Yang, T. McAfee, K. Jiang, Y. Li, Y. Liu, H. Hu, J. Zhao, W. Ma, H. Ade, H. Yan, *Adv. Mater.* **2015**, *27*, 7299.

[40] S. Li, L. Ye, W. Zhao, S. Zhang, S. Mukherjee, H. Ade, J. Hou, *Adv. Mater.* **2016**, *28*, 9423.

[41] W. Zhao, L. Ye, S. Li, X. Liu, S. Zhang, Y. Zhang, M. Ghasemi, C. He, H. Ade, J. Hou, *Sci. China Mater.* **2017**, *60*, 697.

[42] A. Hexemer, W. Bras, J. Glossinger, E. Schaible, E. Gann, R. Kirian, A. MacDowell, M. Church, B. Rude, H. Padmore, *J. Phys.: Conf. Ser.* **2010**, *247*, 012007.

[43] J. Rivnay, S. C. Mannsfeld, C. E. Miller, A. Salleo, M. F. Toney, *Chem. Rev.* **2012**, *112*, 5488.

[44] S. Mukherjee, C. M. Proctor, J. R. Tumbleston, G. C. Bazan, T. Q. Nguyen, H. Ade, *Adv. Mater.* **2015**, *27*, 1105.

[45] E. Gann, A. T. Young, B. A. Collins, H. Yan, J. Nasiatka, H. A. Padmore, H. Ade, A. Hexemer, C. Wang, *Rev. Sci. Instrum.* **2012**, *83*, 045110.

[46] L. Ye, W. Zhao, S. Li, S. Mukherjee, J. H. Carpenter, O. Awartani, X. Jiao, J. Hou, H. Ade, *Adv. Energy Mater.* **2017**, *7*, 1602000.

[47] X. Jiao, L. Ye, H. Ade, *Adv. Energy Mater.* **2017**, *7*, 1700084.

[48] L. Ye, Y. Xiong, S. Li, M. Ghasemi, N. Balar, J. Turner, A. Gadisa, J. Hou, B. T. O'Connor, H. Ade, *Adv. Funct. Mater.* **2017**, *27*, 1702016.

[49] S. Mukherjee, X. Jiao, H. Ade, *Adv. Energy Mater.* **2016**, *6*, 1600699.

[50] Y. S. Sun, E. M. Woo, *Polymer* **2001**, *42*, 2241.

[51] Y. Liu, J. Zhao, Z. Li, C. Mu, W. Ma, H. Hu, K. Jiang, H. Lin, H. Ade, H. Yan, *Nat. Commun.* **2014**, *5*, 5293.

[52] C. Müller, *Chem. Mater.* **2015**, *27*, 2740.

[53] N. Balar, Y. Xiong, L. Ye, S. Li, D. Nevola, D. B. Dougherty, J. Hou, H. Ade, B. T. O'Connor, *ACS Appl. Mater. Interfaces* **2017**, *9*, 43886.

[54] W. Lee, J.-H. Kim, T. Kim, S. Kim, C. Lee, J.-S. Kim, H. Ahn, T.-S. Kim, B. J. Kim, *J. Mater. Chem. A* **2018**, *6*, 4494.

[55] N. Balar, B. T. O'Connor, *Macromolecules* **2017**, *50*, 8611.

[56] S. Wu, *J. Appl. Polym. Sci.* **1992**, *46*, 619.